Spectral and kinetic analysis of thermoluminescence from manganiferous carbonatite

ARTICLE *in* JOURNAL OF LUMINESCENCE · JANUARY 2014

Impact Factor: 2.72 · DOI: 10.1016/j.jlumin.2013.07.047

3 AUTHORS, INCLUDING:

Makaiko Chithambo
Rhodes University
68 PUBLICATIONS **628** CITATIONS
SEE PROFILE

V. Pagonis
McDaniel College
114 PUBLICATIONS **955** CITATIONS
SEE PROFILE

Journal of Luminescence 145 (2014) 180–187

Contents lists available at ScienceDirect

Journal of Luminescence

journal homepage: www.elsevier.com/locate/jlumin

Spectral and kinetic analysis of thermoluminescence from manganiferous carbonatite

M.L. Chithambo [a,*], V. Pagonis [b], F.O. Ogundare [c]

[a] Department of Physics and Electronics, Rhodes University, PO BOX 94, Grahamstown 6140, South Africa
[b] Physics Department, McDaniel College, Westminster, MD 21158, USA
[c] Department of Physics, University of Ibadan, Ibadan, Nigeria

ARTICLE INFO

Article history:
Received 25 April 2013
Received in revised form
12 July 2013
Accepted 16 July 2013
Available online 29 July 2013

Keywords:
Thermoluminescence
Spectra
Manganiferous carbonatite

ABSTRACT

Thermoluminescence spectra of manganiferous carbonatite has been studied from 30 °C to 400 °C over the wavelength range from 200 nm to 800 nm. The natural thermoluminescence appears above 200 °C and shows continuous spectral distribution from 240 nm to 800 nm. Above 500 nm the emission appears in the form of line structure emission. These are reproduced by laboratory irradiation which also produces broad bands near 100 °C. The emission features are attributed to presence of Mn^{2+} impurities in the carbonatite matrix. The spectral study was supplemented by kinetic analysis of the most prominent peaks and their kinetic features are reported.

1. Introduction

Carbonatites are rocks of igneous or metasomatic origin which exist in intrusive or extrusive form [1–3]. The classification of carbonatites has been a recurrent theme in the study of this material and has been based in some cases on the metasomatic nature of the rocks and in others on composition of the mineral [3–6]. The contemporary consensus is that carbonatites should be classified as such if their composition is dominated by carbonate minerals [1]. All carbonates derive from the $(CO_3)^{2-}$ anion and include calcite ($CaCO_3$) and its various isomorphs including magnesite ($MgCO_3$), siderite ($FeCO_3$), rhodochrosite ($MnCO_3$); its polymorph, aragonite and other such forms [6,7].

The number of reports on spontaneous or stimulated luminescence studies of carbonatites is rather meagre and what few exist have been concerned with luminescence properties of admixtures in its carbonates such as calcite, apatite and other examples e.g. [8,9]. Kononova and Tarashchan [10] reported thermoluminescence from α-irradiated carbonates from carbonatites and noted in particular that of samples containing apatite, dolomite and other constituents, the intensity of thermoluminescence from calcite carbonatites exceeded all else. The said high sensitivity of calcite quickly made it an attractive candidate for many applications and the copious literature on calcite spans geological dating [11], medical dosimetry [12] as well as generic defect studies [13–15].

Townsend et al. [16] studied thermoluminescence (TL) spectra of X-ray irradiated natural calcite and its pure habit, Iceland Spar, both with trace manganese impurities and observed most notably, line structures in the emission spectra from the natural calcite. They also reported that the glow-peak near 100 °C, for heating at 2.5 °C s^{-1}, was dominant for low X-ray doses. This study lent support to earlier conclusions e.g. [13,17] that Mn impurities in calcite were putative recombination sites. Townsend et al. [16] referred to Medlin's configurational coordinate diagram for Mn^{2+} ions in calcite [13] and the Orgel energy diagram [18] for free Mn ions to develop an energy level scheme for Mn^{2+} ions in calcite. The significance of the model of Townsend et al. [16] was that the modified transitions better reflected experimental observations than did Medlin's diagram and thereby provided more quantitative evidence of the role of Mn impurities in emission.

Calderon et al. [7] then made an extensive study of 28 different carbonate samples of calcite, dolomite, aragonite and other structural types and drew a number of conclusions some of which should be relevant in understanding luminescence properties of carbonatites. They deduced that Mn impurities are highly efficient recombination sites and that Mn ions in low concentrations result in a variety of narrow band emission whereas at high concentration, broadening of the lowest temperature emission is apparent. The enduring interest in calcite and its various morphologies is exemplified by studies on γ-irradiated limestone [19], its cathodoluminescence under neutron bombardment [20], influence of pressure [21], dose-rate [22] as well as annealing [23] on its luminescence properties and the use of some its features in modelling [24].

* Corresponding author. Tel.: +27 46 603 8450; fax: +27 46 603 8757.
E-mail address: m.chithambo@ru.ac.za (M.L. Chithambo).

0022-2313/$ - see front matter © 2013 Elsevier B.V. All rights reserved.
http://dx.doi.org/10.1016/j.jlumin.2013.07.047

This report is concerned with the spectral and kinetic features of thermoluminescence from X-ray irradiated manganiferous carbonatite. The study is supplemented by kinetic analysis of prominent glow-peaks using the initial-rise and peak shape estimates and glow-curve deconvolution. The emission bands are related to transitions at Mn sites. The aim of the study is to contribute to a better understanding of luminescence properties of carbonatites in general and of the manganiferous varieties in particular.

2. Experimental details

Samples consisted of opaque manganiferous carbonatite from Kangankunde, Machinga, Malawi. The mineral composition of this material has been previously analysed [25] and includes calcite, magnesite, siderite and rhodochrosite as the dominant components as well as various inclusions such as manganese oxides, apatite, monazite and quartz. In this study, the source material was either prepared into thin discs of diameter ~8 mm or milled into powder. Thermoluminescence measurements were made in vacuum, ~1 mbar, at 2.5 °C s^{-1}using a high sensitivity thermoluminescence spectrometer described by Luff and Townsend [26]. Prior to heating, samples were irradiated in-situ with X-rays from a Philips MCN-101 X-ray tube operated at 40 kV/15 mA giving a dose rate of 40 Gy min^{-1}. Preparatory tests using a solid aliquot showed evidence of intense luminescence and consequently 50% transmission filters were used to avoid saturating the light detectors.

The luminescence detection system consisted of a combination of two position-sensitive photomultiplier tubes and two spectrometers capable of recording emissions over the wavelength range 200–800 nm. A diagram of the light collection optics is shown in Fig. 1. Two grating spectrometers and the two position sensitive photomultiplier tubes (imaging photon detectors) were used for spectral analysis and photon counting respectively. The gratings, one at each detector, dispersed the signal across the relevant range i.e. 200–450 nm and 400–800 nm. All spectral data were corrected for the wavelength dependence of the system. 0.5 mm entrance slits were used on the spectrometers giving a typical 5 nm resolution over the whole wavelength range. A 400 nm cut-off filter was permanently inserted in the light path to the 400–800 nm detector to remove the second order scattering of lower wavelengths into the first order spectrum. A spectrum was recorded every 1 s and data subsequently smoothed by using a spectra integration time of 3 s.

3. Results and discussion

3.1. Natural thermoluminescence

Fig. 2 shows the natural thermoluminescence, that is, the signal resulting from accumulated natural irradiation, from a solid aliquot heated at 2.5 °C s^{-1}. The natural TL is seen at temperatures above 200 °C and exhibits a spectral distribution from 240 nm to 800 nm. A broad band of width > 250 nm and centred near 330 nm spans the region 240–520 nm. The apparent reduction in emission near 400 nm could be an experimental artefact caused by a mismatch between the data from the concave gratings since this is the region where they overlap. Above 500 nm the emission is in the form of sharp emission lines near 560, 600 and 700 nm each of average bandwidth of only about 40 nm. Above 750 nm thermal radiation dominates. These features are further clarified in Fig. 3, a composite spectrum produced by summing spectra in the range 300–400 °C. Fig. 4 shows a contour map of the isometric plot shown in Fig. 2. The map shows distinct emission peaks of five glow-curves determined to be at about 340 nm, 558 nm, 594 nm, 640 nm and 700 nm. The corresponding temperature positions of the emission maxima were 356 °C and 364 °C for the emissions at 338 nm and 558 nm and 371 °C for the emissions at 594, 640 and 700 nm.

As mentioned in the previous section, the source material from rocks for use in thermoluminescence measurements were either prepared into thin slices or ground to powder. The effect of

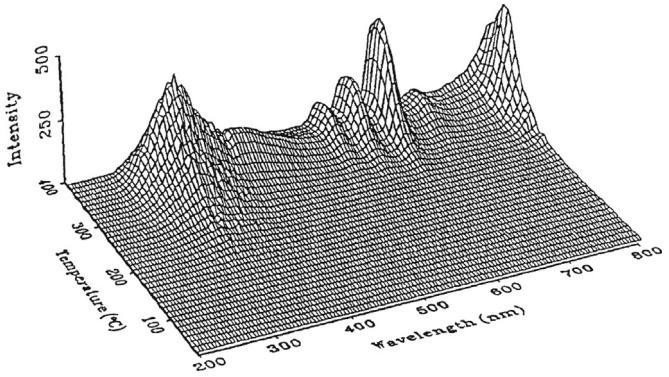

Fig. 2. The natural thermoluminescence of manganiferous carbonatite. Spectra in the range 30–400 °C were recorded every 1 s and the heating rate was 2.5 °C s^{-1}.

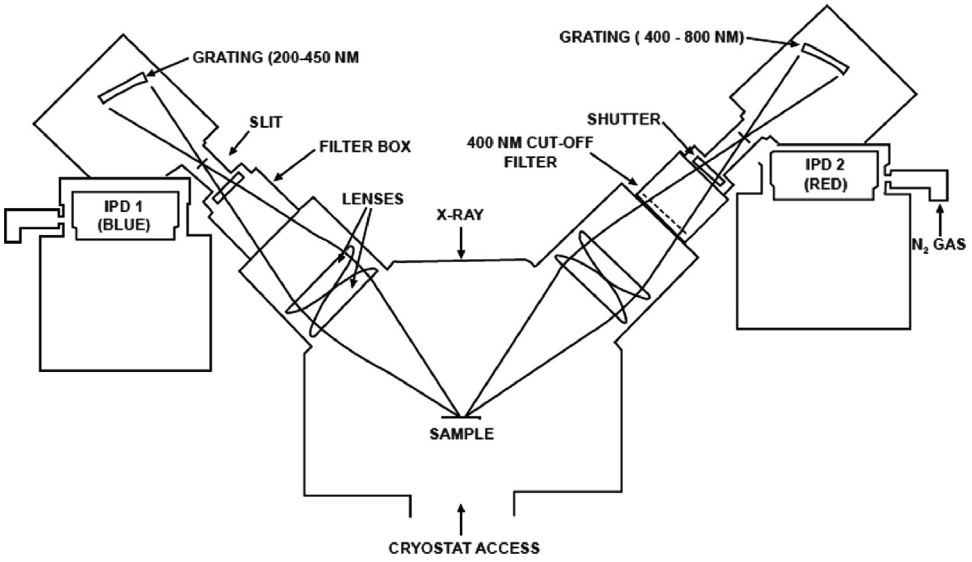

Fig. 1. A schematic diagram of the TL spectrometer. Light is collected by the pair of lenses, dispersed by the pair of grating spectrometers and detected by two position sensitive photomultiplier tubes (IPDs).

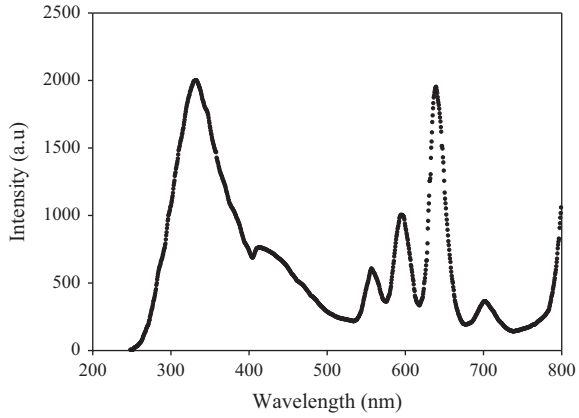

Fig. 3. A composite thermoluminescence spectrum produced by summing spectra in the range 300–400 °C in the data shown in Fig. 2.

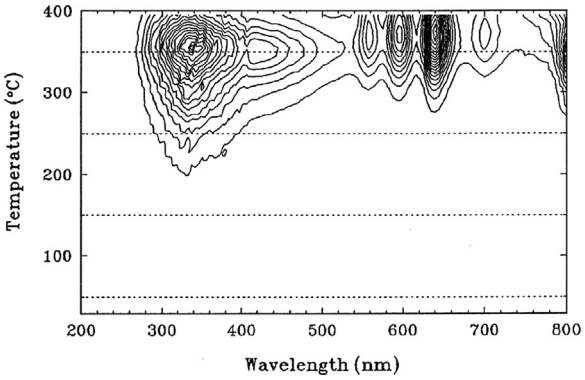

Fig. 4. A contour map of the isometric plot in Fig. 2 showing the temperature dispersion of the luminescence.

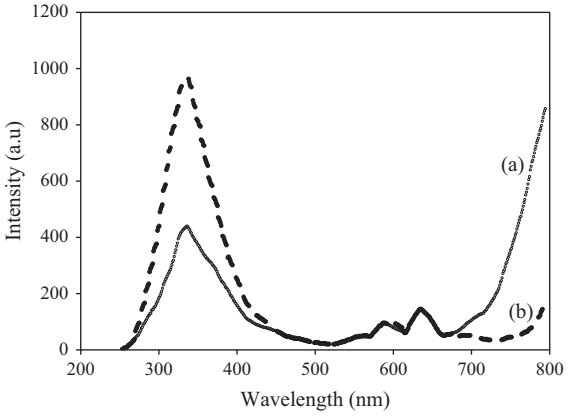

Fig. 5. Comparison of the luminescence intensity from a powdered sample (a; full line) and a solid rock disc (b; dashed line). The intensity of the luminescence from the ground sample has been scaled up by a factor of ~4 to aid visual comparison.

grinding on the thermoluminescence spectra was investigated. Fig. 5 compares TL spectra from thin rock slices (dashed line) and powder samples (solid line) of manganiferous carbonatite. The sensitivity of the TL was seen to be reduced by the powdering. In particular, the peak intensity of the powdered sample is lower than that of the rock slice by factors of ~8 and 4 in the UV–blue and red regions of the spectrum respectively. However, there were no significant spectral changes introduced by the powdering. In view of this, the intensity data for the powdered material has been scaled up to better show the absence of any new spectral bands.

3.2. General features and dose response of laboratory induced luminescence

Laboratory induced thermoluminescence was measured from samples dosed to 800 Gy of X-ray irradiation. It was noticed that spectra measured from X-ray irradiated samples either before or after removal of the natural TL were similar. Fig. 6 shows the isometric plot of an irradiated sample in (a) and the corresponding contour plot in (b). Fig. 6(a) shows a new wide band centred near 650 nm with some evidence of poorly resolved line structures. Further, the emission between 300 and 500 nm is now isolated into at least four glow-curves. In comparison, only the glow-peak above 300 °C is seen in the natural TL (Fig. 2) and is more intense than that induced by 800 Gy of X-ray irradiation in this case. In addition, the intensity of the line structures between 550 and 700 nm, so pronounced in Fig. 2, appears to have significantly decreased with the corresponding glow-peak positions now shifted well above 400 °C. These features are further illustrated in Fig. 6(b) which also clearly shows that the lower temperature emissions below and above 500 nm occur at different temperatures.

Fig. 7 shows the influence of dose on the thermoluminescence from manganiferous carbonatite for X-ray irradiation between 200 through 1400 Gy. The thermoluminescence intensity increases with dose for all four distinct peaks apparent in the glow-curve. However, the nature of the growth curve was examined only for the clearly defined peaks at about 86 and 261 °C and this is shown in Fig. 8. The dose response for both peaks was quantified on the basis of the superlinearity index $g(D)$ and the supralinearity index $f(D)$ given by

$$g(D) = \left[\frac{Dy''(D)}{y'(D)}\right] + 1 \quad (1)$$

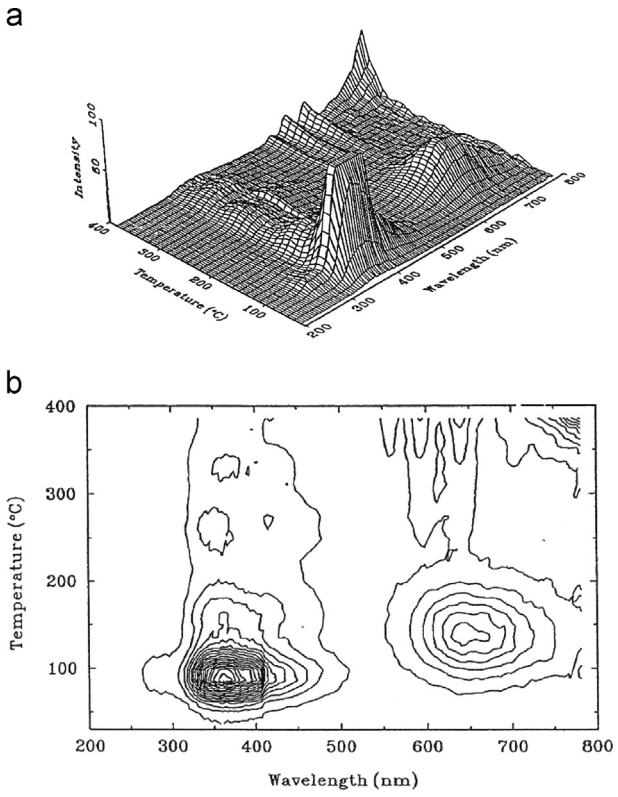

Fig. 6. Thermoluminescence from manganiferous carbonatite irradiated with 800 Gy of X-rays following removal of the natural signal (a) the same data displayed as a contour plot showing in particular the dominant nature of the emission near 90 °C between 300 and 400 nm (b).

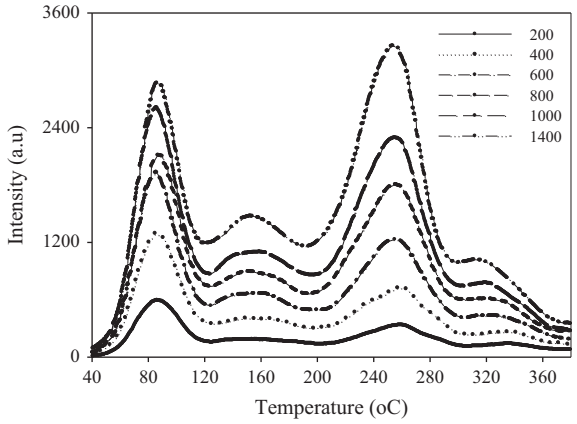

Fig. 7. Increase of thermoluminescence intensity with dose in manganiferous carbonatite.

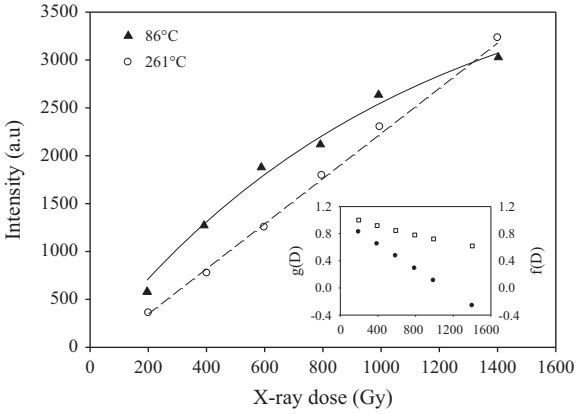

Fig. 8. Dose-response of glow-peaks at 86 °C (upright triangle) and at 261 °C (open circles). The line through data points of the latter is an equation of form $y = mx + c$ whereas the line through data corresponding to the peak at 86 °C is the best fit of Eq. (3). The form of the indices for superlinearity $g(D)$, solid circles, and supralinearity $f(D)$, open squares, for the peak at 86 °C are quantitative evidence that its dose response is sublinear.

and

$$f(D) = \left[\frac{y(D)/D}{y(D_1)/D_1)}\right] \tag{2}$$

where $y(D)$ is the analytical dose dependence of the thermoluminescence intensity, $y'(D)$ and $y''(D)$ are respectively the first and second derivative of $y(D)$ and D_1 is a normalisation dose [27]. The utility of the indices, which have also been discussed in detail elsewhere [28,29], is that $g(D)$ is a measure of the change in slope of the growth curve whereas $f(D)$ is a quantitative measure of deviation from linearity.

The dose response for the peak at ~261 °C is linear as is qualitatively evident from Fig. 8, as can be verified by inspection that $g(D) = 1$, and calculations which showed that $f(D) \sim 1$ throughout the dose range of 200 through 1400 Gy used. On the other hand, analysis of the peak at 86 °C showed that its thermoluminescence intensity is well described as a function of dose as

$$y(D) = A(1 - e^{-bD}) \tag{3}$$

where A (in arbitrary units) and b (in Gy^{-1}) are constants and D is irradiation dose. The solid line through the data points for the 86 °C peak (upside triangles) is the best fit of Eq. (3). The inset to Fig. 8 shows the descriptors $g(D)$ and $f(D)$ for this peak and in particular that both $g(D)$, $f(D) < 1$, quantitative evidence that for the 86 °C peak, the dose response is sublinear throughout the 200–1400 Gy region examined. The index $f(D)$ in the inset can probably be extrapolated to zero suggestive of eventual saturation for this peak at some dose greater than 1400 Gy.

3.3. Electron-trapping characteristics

In order to study kinetic features of electron traps involved in the emission of thermoluminescence, a number of methods including a range of peak position and partial-curve techniques for analysis of the TL peaks for their kinetic parameters were considered. In particular, the variable heating rate method was tried on several samples but was found to be of little use in this study owing to a limited range of heating rates. Further preparatory experimental tests of partial-curve techniques showed that the peaks could be properly analysed using the initial-rise method, peak shape estimates and glow-curve deconvolution.

3.3.1. Initial-rise method

The initial-rise method, discussed comprehensively in several texts e.g. [27,28,30] is based on the approximation that the thermoluminescence intensity I in the rising edge of a TL peak is dependent on temperature T as

$$I(T) = C\exp\left(-\frac{E}{kT}\right) \tag{4}$$

where E is the activation energy, k is Boltzmann's constant and C a constant of proportionality. The expectation then is that for the real experiment data, a plot of $\ln I$ against $1/T$ should be a straight line with slope equal to $-E/k$ from which E can be found. The initial-rise technique is independent of the order of kinetics.

Preparatory to analysis, the overlapping glow-peaks in the TL glow-curve of a sample irradiated to 800 Gy were separated using the thermal-cleaning method described by McKeever [30]. The sample was heated at 2.5 °C s^{-1} successively from 30 °C to and cooled from 100, 180, 280 and 400 °C in order to produce clean rising portions of each glow-peak for use in the initial-rise analysis. Fig. 9 compares a complete glow-curve with results of the thermal cleaning procedure which show four distinct components labelled here as A1, A2, A3 and A4.

The difference in the relative intensity between the component peaks A1, A2, A3 and A4 and the corresponding peaks in the glow-curve in Fig. 9 is an incidental result of experimental treatment. Glow-curve N1 was measured immediately after irradiation. The sample was re-irradiated and stored for 8 days before the thermal-cleaning measurements to resolve the glow-curve into its

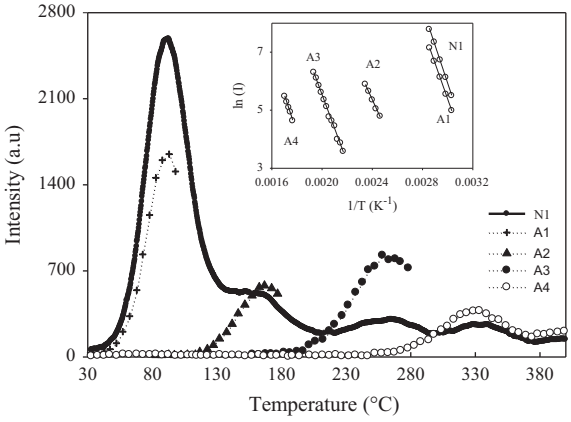

Fig. 9. Successive partial heating from 30 °C to 100, 180, 280, and 400 °C revealed four separate glow-peaks labelled A1, A2, A3 and A4. The original glow-curve N1 is shown for comparison. The dotted lines through data points are only visual guides. The inset shows the initial-rise curves of the data in the main graph. The activation energies deduced in each case are given in Table 1.

components. The delay was initially decided on to reduce the apparent high phosphorescence after the irradiation, a recurrent problem that needed to be dealt with in trying to prevent "swamping" the light detectors. The results show that peak A1 is less intense than the main peak of the original glow-curve N1 (henceforth simply referred to as N1) whereas A2, A3, and A4 are all more intense than the original unresolved glow-peaks. The significant reduction in intensity of peak A1 as compared to N1 is probably caused by fading of the signal between irradiation and measurement. On the other hand, the initial heating to 500 °C after the irradiation before the thermal cleaning procedure seems to have enhanced the sensitivity of peaks A2, A3, and A4. Such an effect has previously been reported but for the red–orange spectral emission in calcite annealed at 500 °C before use [16].

The activation energies were determined from the component peaks using the initial-rise method (inset to Fig. 9). These values were then used to evaluate the frequency factor s using the functional relationship between the heating rate β and activation energy E given by

$$\beta = \frac{SkT_m^2}{E}\exp\left(-\frac{E}{kT}\right) \tag{5}$$

where k is Boltzmann's constant [27,28,30]. The values of the kinetic parameters so found are listed in Table 1. The values of the activation energy for the initial portion of the main peak of glow-curve N1 and its resolved analogue A1 give consistent values of activation energies equal to 0.88 ± 0.04 eV and 0.90 ± 0.04 eV respectively. The activation energies of the correspondingly higher temperature peaks A3 and A4 (1.04 ± 0.03 eV and 1.13 ± 0.09 eV respectively) are greater than for the peaks A1 and A2 (0.90 ± 0.04 eV and 0.77 ± 0.02 eV respectively) at relatively lower temperatures. We also note in Table 1 that peak A1 at 93 °C has a higher value for the activation energy than for curve A2 at 168 °C. A similar analysis was carried out for the glow-peaks corresponding to irradiation-induced line emissions between 550 and 700 nm (see Figs. 2–4) and their corresponding values of E and s are shown in Table 2. In this case, we notice that the ~640 and ~700 nm emission corresponding to the same T_m values have similar values of the activation energy.

Normally it is expected that a deeper trap will empty at a higher temperature. However, the relative positions of glow-peaks are also influenced by a number of other factors including the frequency factor s as well as the recombination and retrapping probability coefficients [28,30,31] and this is relevant in understanding the results of Tables 1 and 2.

Table 1
The activation energy E and frequency factor s for peaks N1, A1 through A4 for temperature positions T_m as listed.

Peak	T_m (°C)	E (eV)	s (s^{-1})
N1	96	0.88 ± 0.04	2.6×10^{11}
A1	93	0.90 ± 0.04	4.9×10^{11}
A2	168	0.77 ± 0.02	7.3×10^{7}
A3	258	1.04 ± 0.03	8.0×10^{8}
A4	322	1.13 ± 0.09	2.3×10^{8}

Table 2
Kinetics values for narrow line emission bands between 550 and 700 nm shown in Figs. 2–4.

T_m (°C)	λ_{max} (± 3 nm)	E (eV)	s (s^{-1})
91	558	1.03 ± 0.02	1.1×10^{7}
98	594	1.09 ± 0.02	2.5×10^{7}
98	640	1.19 ± 0.02	1.7×10^{8}
98	700	1.18 ± 0.04	1.4×10^{8}

3.3.2. Glow-curve deconvolution

In order to provide an independent and complementary assessment of the kinetic analyses, thermoluminescence glow-curves corresponding to various irradiation doses were also analysed using the glow-curve deconvolution method on the basis of general order kinetics. The temperature dependence of the thermoluminescence intensity $I(T)$ is described for general-order kinetics as

$$I(T) = I_m b^{b/b-1}\exp\left(\frac{E}{kT}\frac{T-T_m}{T_m}\right)\left[(b-1)(1-\Delta)\frac{T^2}{T_m^2}\exp\left(\frac{E}{kT}\frac{T-T_m}{T_m}\right)+Z_m\right]^{-b/b-1} \tag{6}$$

where I_m is the peak maximum, T_m the corresponding peak temperature, k Boltzmann's constant, $\Delta = 2kT/E$, $\Delta_m = 2kT_m/E$, and $Z_m = 1 + (b-1)\Delta_m$ [32]. In this method, the activation energy E, the peak-temperature T_m and the order of kinetics b are independent variables that are determined by iteration to a best fit. The frequency factor corresponding to these values were evaluated on the basis of general order kinetics as

$$s = \frac{\beta E}{kT_m^2\left(1+\frac{2kT_m(b-1)}{E}\right)}\exp\left(-\frac{E}{kT}\right) \tag{7}$$

where β is the heating rate and the other kinetic parameters are as previously defined.

Dose dependent measurements in Fig. 7 showed that the glow-curve consists of 4 peaks, affirmed in Fig. 9, and that increasing the dose from 200 Gy to 1400 Gy did not introduce new peaks. Therefore all glow-curves were analysed using a sum of four general order terms of form shown in Eq. (6). Fig. 10 shows a glow-curve measured following an X-ray dose of 400 Gy. The solid line through the data points is the best fit of a sum of four terms of Eq. (6). The four separate peaks determined using deconvolution (dashed and dotted lines) are also shown for completeness. In this example, the order of kinetics b for peak A1 was determined as $b = 2.25 \pm 0.12$, suggestive of second order and the corresponding activation energy as $E = 1.08 \pm 0.02$ eV. The corresponding values

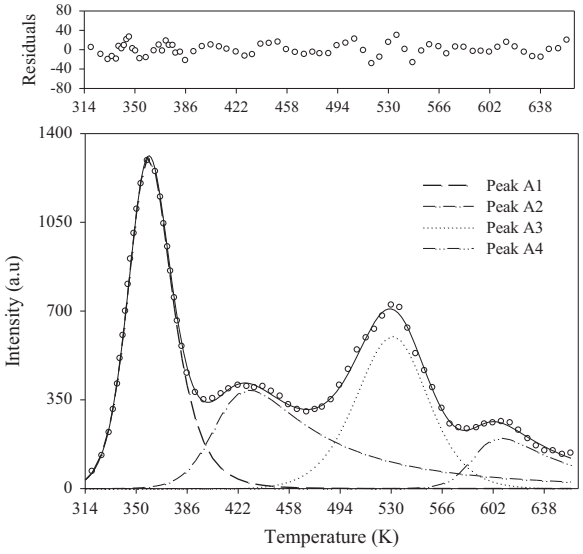

Fig. 10. A glow-curve measured following an X-ray dose of 400 Gy. The solid line through the data points is the best fit of a sum of four terms of Eq. (6). The four separate peaks determined using deconvolution (dashed and dotted lines) are also shown for completeness. The residuals plot, consistent with zero, is evidence of a good fit.

Table 3
Kinetic parameters for peaks A1 and A3 determined using glow-curve deconvolution and the peak-shape procedure.

Method	Peak	Dose (Gy)	E (ev)	b	μ_g	s (s^{-1})
GCD	A1	200	1.10 ± 0.01	2.37 ± 0.03		6.40×10^{14}
		400	1.08 ± 0.02	2.25 ± 0.12		3.35×10^{14}
		600	1.14 ± 0.01	2.31 ± 0.03		2.73×10^{15}
		800	1.05 ± 0.01	2.13 ± 0.04		1.32×10^{14}
		1000	1.11 ± 0.01	2.32 ± 0.03		1.16×10^{15}
		1400	0.91 ± 0.01	1.46 ± 0.04		1.19×10^{12}
	A3	200	1.66 ± 0.02	1.97 ± 0.04		4.80×10^{14}
		400	1.21 ± 0.12	1.63 ± 0.23		3.95×10^{10}
		600	1.28 ± 0.02	1.63 ± 0.05		2.39×10^{11}
		800	1.02 ± 0.02	1.08 ± 0.06		5.57×10^{8}
		1000	1.15 ± 0.02	1.30 ± 0.03		1.07×10^{10}
		1400	0.89 ± 0.03	0.99 ± 0.05		3.30×10^{7}
PS	A1	–	0.91 ± 0.05[a]		0.53 ± 0.01[d]	
		–	1.00 ± 0.06[b]			
		–	1.05 ± 0.04[c]			
	A3	–	1.14 ± 0.36[a]		0.47 ± 0.04[d]	
		–	1.20 ± 0.37[b]			
		–	1.31 ± 0.37[c]			

[a] E_ω.
[b] E_τ.
[c] E_δ.
[d] Values of μ_g apply for E_ω, E_τ and E_δ. Only average values are listed here.

for peak A3 were found to be $b=1.63 \pm 0.23$ and $E=1.21 \pm 0.12$ eV. These results compare favourably with findings from the initial-rise method shown in Table 1 for peaks A1 and A3 respectively namely 0.90 ± 0.04 eV and 1.04 ± 0.03 eV although the data in the latter are for a sample irradiated to 800 Gy. The complete set of values of the activation energy E, order of kinetics b and the frequency factor s for peaks A1 and A3, the most well defined of the four peaks, as determined using glow-curve deconvolution is shown in Table 3.

3.3.3. Peak-shape method

The calculations using glow-curve deconvolution were augmented by use of Chen's peak shape method. In this well-discussed geometrical procedure [27,28,30], the activation energy E_γ can be estimated in one of three possible ways as

$$E_\gamma = C_\gamma\left(\frac{kT_m^2}{\gamma}\right) - b_\gamma(2kT_m) \tag{8}$$

Finding the options for the activation energy requires, for each peak, use of its full width at half-maximum ω, at lower half width τ and upper half width δ. The order of kinetics b can then be deduced from its relationship to the so called geometrical factor $\mu_\gamma=\delta/\omega$. The constants C_γ are given by

$$C_\tau = 1.51 + 3.0(\mu_g - 0.42), \quad b_\tau = 1.58 + 4.2(\mu_g - 0.42); \tag{9}$$

$$C_\delta = 0.976 + 7.3(\mu_g - 0.42), \quad b_\delta = 0; \tag{10}$$

$$C_\omega = 2.52 + 10.2(\mu_g - 0.42), \quad b = 1. \tag{11}$$

Calculations of the activation energy and the geometrical factor did not show any systematic influence due to dose and as such only average values of E_ω, E_τ and E_δ are listed in Table 3 for results from the peak-shape method. Values of E_γ for example $E_\omega=0.91 \pm 0.05$ eV, are consistent with values of E found using the initial-rise and glow-curve deconvolution methods. Of particular interest however is that for peak 1, $\mu_g=0.53 \pm 0.01$, indicative of second order kinetics, in good agreement with the various examples of b determined using glow-curve deconvolution. The corresponding value for peak 3, $\mu_g=0.47 \pm 0.04$, implies kinetics intermediate between 1 and 2 as can be deduced from the reference parameters of Chen (McKeever [30], his Fig. 3.13). A similar feature is also apparent for peaks 1 and 3 in the results from glow-curve deconvolution although reasons for the exceptions in b, for peaks corresponding to 200 and 1400 Gy are not immediately obvious.

Previous kinetic analyses on calcite, the supposed dominant component of carbonatite, showed glow-curves with 4 sometimes 5 peaks depending on irradiation dose, type, heating rate and other factors e.g. [33,34]. A direction comparison of values in this study with those in the literature may be specious but nevertheless some general observations can be made.

The first peak in calcite, the so called 80 °C peak, was interpreted by Medlin [35] as being due to localised transitions and assigned $E=0.75$ eV. The same peak was studied by Visocekas et al. [36,37] who ascribed its nature to a distribution of values of the frequency factor s and set $E=0.62$ eV. In further studies, Kirsh et al. [34] confirmed the notion of a distribution of energy levels and reported $E=0.73$ eV with a distribution of s values. Pagonis et al. [38] in a study on UV irradiated calcite reported $E=0.78 \pm 0.03$ eV and $s=(1-7)x\ 10^{10}\ s^{-1}$. Concerning the peak referred to as A3 in this report, the values, say, 1.02 ± 0.02 eV (Table 3, 800 Gy, peak A3) may be compared with 1.1 eV [33] or 1.02 eV [34] or 1.50 eV [39]. In general, our values for E for peak 1 are less than the literature ones. There may be a number of reasons for this principally that the material studied for this work is carbonatite rather than pure calcite and this may have a bearing on the electron traps and their associated activation energy.

3.4. Spectral emission features

The natural thermoluminescence measured at high temperature (>300 °C) as shown in Fig. 2 is evidence that deep charge traps are involved. Activation energies of the order of 1.0 eV and greater for the main peak of glow-curve N1 (Table 1) and the line structure emission (Table 2) attest to this. Defects which provide the charge traps are activated at temperatures from 30 °C to well above 400 °C in the X-ray induced TL (Fig. 6) whereas glow-peaks below 300 °C are absent in the natural TL. It is likely then that the lower temperature peaks are unstable over the geological time scales of the carbonatite. To examine this further, it is instructive to compare the age of the carbonatite in this study, 123 ± 6 Ma [40] with an estimate of the lifetime t of a typical electron trap as can be abstracted from the equation

$$N/N_0 = s\exp\left(-\frac{E}{kT}\right) \tag{12}$$

where E is the activation energy, s is the frequency factor, N is the number of traps at time t and N_0 is the original number of traps and the ratio N/N_0 is proportional to the ratio of the natural and laboratory-induced peak intensities [14,41]. Using values for the 700 nm narrow band in Table 2 and taking $T=300$ K as ambient temperature for an extrusive rock, one finds in this case that $t \cong 2{,}00{,}000$ years $\ll 123$ Ma. Thus it is apparent that the TL is from traps that are fairly recent in comparison with the age of the rock. This implies that defects that provide the electron traps are continually subjected to annealing and subsequent refilling over time.

The thermoluminescence emission features of carbonatites are complex and cannot each be unambiguously identified against each constituent of the material. Indeed, manganiferous carbonatite studied in this work is a natural agglomeration of various components including monazite, strontianite, calcite, barytes, oxides and rare earth elements [1,42]. Many of the constituent minerals are luminescent [43]. Rather less known is that strontianite from the same ore as the carbonatite is reported to have given off ~589 nm thermoluminescence at about 100 °C [25] in

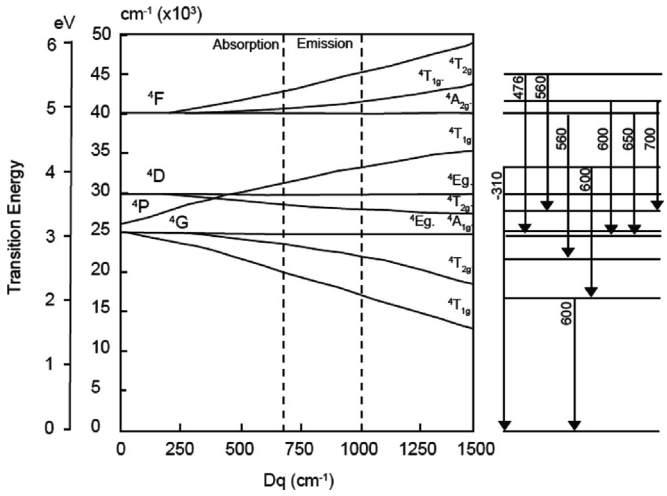

Fig. 11. Electronic transitions for luminescence in Mn^{2+} in calcite shown alongside the corresponding Orgel diagram as revised by Calderon et al. [7].

experiments no less serendipitous than the 1663 account of Boyle [30]. However, it is reasonable to assume that some prominent luminescence features in carbonatites are due to calcite, its most dominant component.

Thermoluminescence in calcite is attributed to presence of Mn^{2+} impurities which act as recombination sites and give at low concentration, line structure- and at high concentration broad-band features [7,16]. The emission of luminescence from Mn^{2+} may be discussed with respect to transitions between its energy levels. The energy levels of a free Mn^{2+} ion are however distorted for an Mn^{2+} ion embedded in calcite, where it substitutes for Ca with the magnitude of the change being subject to the metal-ligand bond length in various calcite polymorphs. The resultant Orgel diagram [18] using which Calderon et al. [7] calculated a set of electronic transitions for Mn^{2+} in calcite is shown in Fig. 11.

There are some important similarities in the spectra of manganese doped calcite and manganiferous carbonatite. For example the results of Down et al. [17] show line structure emission at 425 °C for X-ray irradiated calcite. The wavelengths of these lines are given as 560, 600, 640, and 705 nm. Calderon et al. [7] reported emissions at 310, 476, 560, 600, 650 and 700 nm. In comparison, in the natural TL of Mn-carbonatite, the line emissions are near 560, 600, 640 and 700 nm seen near 370 °C. In X-ray data, the line emissions are truncated in mid-increase at 400 °C (Fig. 6a). Calcite TL also shows two broad-bands centred near 650 [7]. In contrast, X-rays did not excite any blue TL in calcite e.g. see Calderon et al. [7] as was the case in manganiferous carbonatite.

Although precise transitions for Mn^{2+} in manganiferous carbonatite are yet to be reported, certain propositions can be made with respect to Mn^{2+} and its known transitions in calcite, the dominant component of the carbonatite. The line emission at 594 nm in manganiferous carbonatite is assumed to be the same primary electronic transition from the ^4G (T_{1g}) level to the ground state, ^6S in calcite [7,16,17,37]. The emissions at 558 and 700 nm are consistent with ^4F (T_{2g})→^6S and ^4F (T_{1g})→^6S transitions respectively. We assume that the line structure at 640 nm is a modified version of the ^4F→^4G transition in calcite although a similar emission is in other cases attributed to the ^4F (T_{1g})→^6S transition in aragonite [7]. The emission between 200 and 500 nm might be due to another impurity.

Regarding the presence of broad emission bands, it is thought that at high concentration the Mn^{2+} ions cluster into pairs or trimers. The local ion energy states overlap and the resulting emission appears as a wide band [17]. In Fig. 6(a) the band shows some evidence of line emission in the broad-band near 650 nm although to clearly resolve these, a grating of dispersion better than the 6 nm/mm would be needed. At high temperature, during heating, the Mn^{2+} clusters dissociate into isolated Mn^{2+} centres and it is these acting as emission centres that are responsible for the clearly resolvable emission lines as seen in Fig. 2 with specific transitions as discussed above. The spectroscopic and luminescence features of Mn^{2+} have otherwise also been discussed in detail elsewhere [44–46].

4. Conclusion

Thermoluminescence spectra of manganiferous carbonatite has been studied from 30 °C to 400 °C over the wavelength range from 200 nm to 800 nm. The natural TL appears above 200 °C and shows continuous spectral distribution from 240 nm to 800 nm. Above 500 nm the emission is in the form of narrow band emission. The line structures are reproduced by laboratory irradiation which also produces broad bands near 100 °C. The emission features are attributed to transitions at Mn^{2+} ion impurities in the carbonatite. The spectral study was supplemented by kinetic analysis of the most prominent peaks and their kinetic parameters have been given.

Acknowledgements

MC is grateful to the British Council under whose auspices this work was carried out, to Rhodes University and the National Research Foundation for financial support, to the Geological Survey Department, Zomba, Malawi, for the carbonatite sample and to Prof Peter Townsend of the University of Sussex for much.

References

[1] A.R. Wooley, Alkaline Rocks and Carbonatites of The World part 3: Africa, The Geological Survey of London, London, UK, 2001.
[2] A.R. Wolley, The spatial and temporal distribution of carbonatites, in: K. Bell (Ed.), Carbonatites: Genesis and Evolution, Chapman and Hall, London, UK, 1989.
[3] A.R. Wooley, D.R.C. Kempe, Carbonatites: nomenclature, average chemical compositions, and element distribution, in: K. Bell (Ed.), Carbonatites: Genesis and Evolution, Chapman and Hall, London, UK, 1989.
[4] R.H. Mitchell, Can. Mineral. 43 (2005) 2049.
[5] Y.L. Kapustin, Accessory Rare Metal Mineralization of The Carbonitites of The Kola Peninsula, Nauka Press, Moscow, 1964.
[6] C.D. Gribble, Rutley's Elements of Mineralogy, 27th ed., Unwin Hyman, London, 1988.
[7] T. Calderon, P.D. Townsend, P. Beneitez, J. Garcia-Guinea, A. Millan, H.M. Rendell, A. Tookey, M. Urbina, R.A. Wood, Radiat. Meas. 26 (1996) 719.
[8] U. Kempe, J. Götze, Mineral. Mag. 66 (2002) 151.
[9] A.N. Zaitsev, A.R. Chakhmouradian, Can. Mineral. 40 (2002) 103.
[10] V.A. Kononova, A.N. Tarashchan, Internat. Geol. Rev. 12 (1970) 272.
[11] A.J. Wintle, Can. J. Earth. Sci. 15 (1978) 1977.
[12] H.Y. Gosku, A. Wieser, A. Waibel, A. Vogenauer, D.F. Regulla, Appl. Radiat. Isot. 40 (1989) 905.
[13] W.L. Medlin, in: D.J. McDougall (Ed.), Thermoluminescence of Geological Materials, Academic Press, London, 1968.
[14] P.D. Townsend, in: D.J. McDougall (Ed.), Thermoluminescence of Geological Materials, Academic Press, London, 1968.
[15] R. Visocekas, Euro.PACT. 23 (1979) 258.
[16] P.D. Townsend, B.J. Luff, R.A. Wood, Radiat. Meas. 23 (1994) 433.
[17] J.S. Down, R. Flower, J.A. Strain, P.D. Townsend, Nucl. Tracks 10 (1985) 581.
[18] L.E. Orgel, J. Chem. Phys. 23 (1955) 1004.
[19] V. Ponnusamy, V. Ramasamy, M.T. Jose, K. Anandalakshmi, J. Lumin. 132 (2012) 1063.
[20] D.K. Silletti, S.A. Brokus, E.B. Earlywine, J.D. Borycz, G.F. Peaslee, P.A. DeYoung, N.J. Peters, J.D. Robertson, J. Buscaglia, Radiat. Meas. 47 (2012) 195.
[21] A.R. Lakshmanan, Radiat. Meas. 39 (2005) 235.
[22] R.M. Martin, J.L. Brady, A.M. Lew, M. Urbina, A. Millan, P. Beneitez, T. Calderon, J. Lumin. 79 (1998) 21.
[23] V. Pagonis, M. Christodoulos, Radiat. Meas. 23 (1994) 131.
[24] R. Chen, J.L. Lawless, V. Pagonis, Radiat. Meas. 46 (2011) 1380.
[25] D.N. Holt, The Kangankunde Hill Rare Earth Prospect, Govt. Press, Zomba, Malawi, 1965.

[26] B.J. Luff, P.D. Townsend, Meas. Sci. Technol. 4 (1993) 65.
[27] V. Pagonis, G. Kitis, C. Furetta, Numerical and Practical Exercises in Thermoluminescence, Springer, New York, 2006.
[28] R. Chen, S.W.S. McKeever, Theory of Thermoluminescence and Related Phenomena, World ScientificSingapore, 1997.
[29] R. Chen, S.W.S. McKeever, Radiat. Meas. 23 (1994) 667.
[30] S.W.S McKeever, Thermoluminescence of Solids, Cambridge University Press, Cambridge, 1985.
[31] P.D. Townsend, J.C. Kelly, Colour Centres and Imperfections in Insulators and Semiconductors, Chatto and Windus, London, 1973.
[32] G. Kitis, J.M. Gomes-Ros, J.W.N. Tuyn, Appl. Phys. 31 (1998) 2636.
[33] V. Pagonis, C. Michael, Radiat. Meas. 23 (1994) 131.
[34] Y. Kirsh, P.D. Townsend, S. Shoval, Nucl. Tracks Radiat. Meas. 13 (1987) 115.
[35] W.L. Medlin, Phys. Rev. 75 (1964) A1770.
[36] R. Vicosekas, T. Ceva, F. Lefauchex, M.C. Robert, Phy. Stat. Sol. 35a (1976) 515.
[37] R. Vicosekas, A. Geoffroy, Phys. Stat. Sol. 41a (1977) 499.
[38] V. Pagonis, E. Allman, A. Wooten Jr, Radiat. Meas. 26 (1996) 265.
[39] V. Pagonis, C. Shannon, Radiat. Meas. 32 (2000) 805.
[40] L. Cahen, N.J. Snelling, The Geochronology of Equatorial Africa, North-Holland Publishing Company, Amsterdam, Holland, 1996.
[41] M.J. Aitken, Introduction to Optical Dating, Oxford University Press, Oxford, UK, 1998.
[42] M.S. Garson, Carbonatites and Agglomeratic Vents in the Western Shire Valley, Geological Survey of Malawi, Zomba, Malawi, 1965.
[43] M. Gaft, R. Reisfeld, G. Panczer, Modern Luminescence Spectroscopy of Minerals and Materials, Springer-Verlag, Berlin, 2005.
[44] A. Padmanabham, T. Satyanarayana, Y. Gandhi, N. Veeraiah, Phys. Status Solidi A 207 (2010) 80.
[45] N. Krishna Mohan, M. Rami Reddy, C.K. Jayasankar, N. Veeraiah, J. Alloys Compd. 458 (2008) 66.
[46] G. Venkateswara Rao, P. Yadagiri Reddy, N. Veeraiah, Mater. Lett. 57 (2002) 403.